https://doi.org/10.3311/PPch.19730

Periodica Polytechnica Chemical Engineering, 66(4), pp. 585–595, 2022

High Surface Area Silica Particles Using Anionic Surfactant Template Prepared by One-step Spray Drying System for Dye Removal Application

Hendrix Abdul Ajiz[1], Abdurrahman Anis Albar[1], W Widiyastuti[1*], Tantular Nurtono[1], Heru Setyawan[1], I Made Joni[2]

[1] Department of Chemical Engineering, Faculty of Industrial Technology and Systems Engineering (INDSYS), Institut Teknologi Sepuluh Nopember, Kampus ITS Sukolilo, Surabaya 60111, Indonesia
[2] Department of Physics, Faculty of Mathematics and Natural Sciences (FMIPA), Universitas Padjadjaran, Jl. Raya Bandung-Sumedang km. 21, Jatinangor 45363, Indonesia
[*] Corresponding author, e-mail: widi@chem-eng.its.ac.id

Received: 21 December 2021, Accepted: 31 March 2022, Published online: 20 May 2022

Abstract

This study reported the effect of sodium lauryl sulfate (SLS) as a template on silica morphology and its properties. The precursor was prepared by producing silica nanofluid by the sol-gel method and mixed with various SLS concentrations. After that, the precursor was spray-dried to generate silica powder. An increase in SLS concentration up to 2 critical micelle concentration (CMC) indicates an increase in the silica particle size from 2.12 μm in untemplated silica particles to 2.58 μm. On the other hand, when the SLS concentration increases to 3 CMC, the particle size decreases to 2.19 μm. A significant increase in total pore volume and surface area is obtained for silica particles synthesized at least at the SLS concentration of 2 CMC, around eight higher volumes than without SLS addition. In addition, they have a macropore compared to silica particles synthesized without SLS addition that only exhibits mesopore. The surface area was 1,011 m^2/g for the SLS concentration at 3 CMC, whereas the silica without SLS has only a surface area of 131 m^2/g. The SLS concentration at 2 CMC or higher leads to a significant increase in its physical properties because the micelle formation is enough for sacrificed template formation. Methylene blue solution was used as an adsorbate for evaluating the dye adsorption capacity that followed the Langmuir isothermal adsorption model. The highest theoretical maximum monolayer adsorption capacity was 142.9 mg/g, obtained by silica adsorbent with the SLS concentration at 3 CMC.

Keywords

aerosol, adsorbent, macro-mesoporous particles, silica nanofluid, spray dryer

1 Introduction

Silica particles have many applications, from liquid and gas waste processes, to overcome the energy problem [1–6]. Silica particle morphology has an essential role in supporting its performance in different applications. Silica can be obtained from commercial materials such as tetraethyl orthosilicate (TEOS), tetrakis (2-methoxyethyl) orthosilicate (TMEOS), or extracted from biomass waste containing silica [7–10]. Controlling silica particles' morphology differs from one silica source to another. Silica sourced from TEOS has the advantage of a relatively slow reaction, so it is easy to control, but the high price of TEOS makes it less economical. One source of silica that is cheap and easy to obtain is sodium silicate. However, controlling the morphology of silica sourced from Sodium silicate has its challenges because the polymerization and condensation reactions are speedy. Therefore, selecting the right conditions is necessary to obtain silica particles with the desired morphology [11, 12]. Various methods have been proposed to synthesize silica particles. There are many promising methods for synthesizing silica particles, including liquid processes such as sol-gel, emulsion, and aerosol methods [13–16]. The aerosol method is more effective because the time required is relatively short than other methods [17, 18]. Silica can be generated by aerosol processed such as flame spray drying [19], spray drying [8], and spray drying in a tubular furnace [20].

Cite this article as: Ajiz, H. A., Albar, A. A., Widiyastuti, W., Nurtono, T., Setyawan, H., Joni, I. M. "High Surface Area Silica Particles Using Anionic Surfactant Template Prepared by One-step Spray Drying System for Dye Removal Application", Periodica Polytechnica Chemical Engineering, 66(4), pp. 585–595, 2022. https://doi.org/10.3311/PPch.19730

One technique for controlling silica morphology is to increase the porosity of the particles and control the particle diameter in narrow size distribution [21, 22]. One way that can be used is to add a template to the silica matrix. The template is a material that can be used as a mold to form a specific structure on silica particles. Usually, the template that is widely used comes from polymer compounds [23–25] or inorganic compounds such as ZnO, which can be removed by acid dissolving [16, 26]. Macropore silica was successfully synthesized with a polystyrene latex (PSL) template using an ultrasonic spray dryer with two drying stages: low temperature around 120–200 °C to form hybrid particles and high-temperature 600 °C to remove the template. From these results, the morphology of the formed particles has two forms, namely hollow and porous particles. The two types of morphology are different due to the zeta potential value differences. The increase in silica concentration also causes an increase in the diameter of the porous particles [21, 25]. Besides producing macroporous silica in one step simultaneously with the template removal process, the use of spray drying can also produce inert coated silica particles in the microencapsulation process with high particle stability [27].

In addition to using polymers, other materials that can be used as templates are surfactants. Surfactant is a compound with a different polarity, hydrophilic at the head with a hydroxyl group (–OH) and hydrophobic at the tail composed of carbon chains [28]. The size and morphology of the silica particles can be controlled by using the emulsion method with surfactant. Lee et al. [14] controlled the size and morphology of silica particles using non-ionic surfactants and sodium silicate as silica sources. A uniform particle size distribution in the submicron to micron range can be obtained with spherical morphology and sodium-free using the water/oil emulsion method. Zhang et al. [15] synthesized silica/polystyrene composites using the mini emulsion polymerization method with anionic surfactant sodium lauryl sulfate (SLS) as a droplet stabilizer in the emulsion. The mini emulsion formation process is carried out in several stages, including modifying the silica surface to be hydrophobic using methacrylate (propyl) trimethoxysilane (MPS), followed by the formation of silica/polystyrene composites in a mini emulsion polymerization system. These results obtained core-shell particle morphology with silica particles embedded in monomer droplets [15]. From the morphology and particle size produced using the emulsion method, it is shown that surfactant is one of the essential parameters that can be used to produce controlled particle morphological characteristics. However, the silica particle synthesis process's emulsion system method is limited to particle morphology but has not shown a pore control mechanism to produce morphological characteristics as a porous material.

Ionic and non-ionic surfactants have different mechanisms in controlling particle size based on the hydrophilic group's charge and the particle's charge. Different types of particles such as gold and silica will have different charge values, so certain types of surfactants are needed to produce stable electrostatic interactions [29]. Generally, in synthesizing silica particles, the concentration and type of surfactant charge will affect the size and morphology of the particles. Silica particle size will increase with increasing surfactant concentration. Due to the availability of abundant carboxylic acids and hydroxyl groups, it can increase the bonding of the nanoparticle surface through hydrogen bonds in non-ionic surfactants and weaken the van der walls and electrostatic forces on ionic surfactants. Both mechanisms can induce aggregation at higher surfactant concentrations [30, 31]. On the other hand, surfactants can also be used as a template to control the pore size of the silica particles. The mesoporous silica was successfully synthesized using Cetyltrimethylammonium bromide (CT-MABr) cationic surfactant as template and TEOS as a silica source [32]. The specific surface area of mesoporous silica particles increased with the surfactant concentration. However, the post-treatment was needed using a hydrothermal process to increase and stabilize the formed pores. In an acidic environment, the synthesis of mesoporous silica from sodium silicate can also be carried out with the template from an anionic surfactant, sodium dodecyl sulfate (SDS). The surfactant template was removed at a high temperature as a separate stage. The obtained mesoporous silica had a surface area of 630 to 1,403 m^2/gr [33]. The surfactant template on the silica particles can also be removed by using the extraction method with a particular solvent to remove the template [34]. However, it has been reported that the removal process of silica particle template by heating or extraction methods can cause a decrease in surface area and structural damage of the generated particles caused by excessive-high temperatures and a prolonged period process [35, 36].

Most previous research is still limited to two separate process stages: particle formation and template removal. Therefore, we report a one-step method to generate a high surface area of silica particles for particle formation and template removal in a spray dryer with a relatively short

residence time and low temperature. Sodium silicate is selected as a silica source and the anionic surfactant of sodium lauryl sulfate (SLS) as the template. The surfactant concentration is varied to investigate the effect of surfactant concentration on the generated particle characteristics. In addition, the performance of the generated silica particles as a dye adsorbent is also analyzed.

2 Materials and methods

2.1 Materials

Sodium lauryl sulfate (SLS) as an anionic surfactant in technical grade was purchased from CV. Citra Sari Kimia, Indonesia. Sodium silicate with SiO_2 content of 28%, SiO_2: Na_2O = 3.3 was received from PT. PQ Silicas Indonesia. The other chemicals used Flotrol-007 cationic resin, potassium hydroxide p.a. Merck, and 37% hydrochloric acid p.a. Mallinckrodt. Methylene blue in technical grade for analyzing the ability of silica adsorbent was purchased from UD. SIP, Indonesia. All chemicals were used without further purification. The water used in the synthesis process is demineralized water purchased from UD. SIP, Indonesia.

2.2 Particle synthesis

The synthesis of silica nanofluid has been reported by previous research [37]. Briefly, an ion exchange process using Flotrol-007 cationic resin to obtain an active silicic acid solution at pH 2 carried out the sodium silicate solution of 0.3 M. Then, 0.1 M KOH solution was added drop by drop to the silicic acid solution till the pH was 8 to produce silica nanofluid. Finally, SLS was added into the silica nanofluid with concentrations varied from 0.5 to 3 of critical micelle concentrations (CMCs) to generate surfactant-silica nanofluid used as a precursor in the spray drying system (TFS-2L, China) to generate silica particles. First, the spray drying was operated using heating air temperature and flow rate of 200 °C and 414 L/min, respectively, and the feed rate of the precursor was controlled at 5 mL/min.

2.3 Characterization

The concentration of SLS surfactant added to the silicate matrix is based on the CMC value obtained from the correlation between SLS concentration and their surface tension in water. The surface tension of the SLS solution was measured by Du-Nouy ring CSC-70535. The silica particle's surface area and pore volume were quantitatively determined using the nitrogen isotherm adsorption-desorption method (NOVA 1200, Quantachrome). Before the analysis, silica particles were degassed at 300 °C under nitrogen gas for 3 hours. The area was determined by the Braunauer-Emmett-Teller (BET) method at a relative pressure of <0.3, while the pore volume was calculated from the adsorption-desorption profile data of the isothermal desorption branch using Barret-Joyner-Halenda (BJH) at the relative pressure close to 1.0. Scanning Electron Microscopy (SEM) analyzed the silica particle's morphology with Hitachi FlexSEM 1000. The SEM images were processed with ImageJ software to determine the size distribution of the silica particles produced using at least 200 particles. In addition, Fourier Transform Infrared Spectroscopy (FTIR; Thermo Scientific Nicolet iS10) aimed to determine the functional groups in the precursor solution and silica particles. FTIR analysis was performed with an infrared wavenumber of 400–4000 cm^{-1}. The crystallinity of silica particles was determined by X-Ray Diffraction (XRD; PANalytical, X'Pert Pro, Netherlands).

2.4 The performance of silica particles as adsorbent for dye sorption

The ability of silica particles without and with surfactant templates as dye adsorbents were carried out in batches process by using methylene blue solution as the adsorbate. Determination of the isothermal adsorption capacity of the silica adsorbent was carried out using various concentrations of adsorbate solution with a fixed volume of 10 mL. The weight of the silica adsorbent for each adsorbate was 12 mg. The suspension was then homogenized for 5 hours using a shaker. The determination of the equilibrium capacity of the methylene blue (Q_e) adsorbs in mg/g is expressed in Eq. (1):

$$Q_e = \frac{(C_i - C_e)V}{m}, \tag{1}$$

where C_i is the initial concentration of methylene blue, C_e is the equilibrium concentration after adsorbs, V is the volume of the adsorbate, and m is the mass of the silica adsorbent used in the adsorption process. After the adsorption process and the equilibrium state was achieved, the concentration of the methylene blue solution was measured using a UV-Vis spectrophotometer (West tune, N2S) at a wavelength of 664 nm. The data from the adsorption experiment is then fitted with the Langmuir model to estimate the adsorption mechanism. The Langmuir equation is:

$$\frac{C_e}{Q_e} = \frac{1}{Q_m k} + \frac{C_e}{Q_m}, \tag{2}$$

where Q_m is the theoretical maximum monolayer adsorption capacity (mg/g), and k is the Langmuir constant.

3 Results and discussion

The particle size distribution of silica nanofluid as a precursor before being sprayed in a spray drying system had an average diameter of 3.51 nm, as shown in Fig. 1. The homogenous particle size was indicated by the geometric standard deviation of 1.26. After the silica nanofluid was spray-dried, the generated particle size followed the droplet size that evolved the solvent evaporation. As a result, the donut-like particles were formed, as shown in Fig. 2 (a). The average size and the geometric standard deviation were 2.12 μm and 1.49, as shown in Fig. 2 (b).

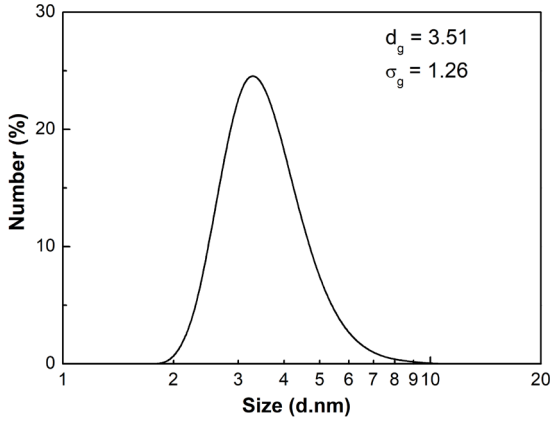

Fig. 1 Particle size distribution of silica nanofluid

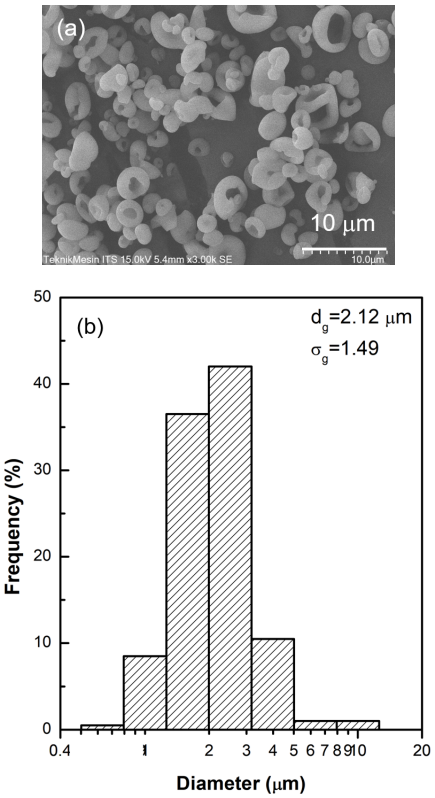

Fig. 2 (a) The SEM image and (b) the particle size distribution of silica particles without SLS template

The micrometer size in dried particles because the formation of the particles follows one droplet to one particle in the spray drying system. The water evaporation from the droplet surface exposes the nanoparticles at the liquid-vapor interface, which shrinks into the vapor phase. Because the solid-vapor interface's surface energy is greater than that of the liquid-vapor interface, the nanoparticles migrate towards the center of the droplet to minimize surface energy. As a result, the fast convective drying rate at the evaporation of water is shorter than the time required for the nanoparticles to diffuse back into the center of the droplet, resulting in a donut-like morphology.

Before the effect of SLS addition on the generated template was studied, the equivalent SLS concentration for a CMC was examined. The SLS CMC in water was determined by measuring the surface tension at various SLS concentrations based on ASTM D1331. As shown in Fig. 3, the intersection of two slopes resulted in the SLS CMC approximately at an SLS concentration of 600 mg/L H_2O.

The morphology and the size distribution of the particles synthesized by SLS addition are shown in Figs. 4–7. Fig. 4 (a) shows the morphology of the silica particles with SLS addition at 0.5 CMC. SLS addition at a concentration below the CMC resulted in the particles with the donut-like morphology, same as the generated particles without SLS addition. Although the morphology of particles did not show a significant change, the average geometric size increased to 2.39 μm compared to particles without SLS addition that had 2.12 μm. Fig. 5 (a) shows the morphology of silica particles at an SLS concentration of 1 CMC. A change in wall thickness is thinner than silica particles with the addition of SLS concentration below the CMC value. Although the wall thickness changes, the particle diameter tends to be constant at 2.39 μm, having the same average geometric size as the

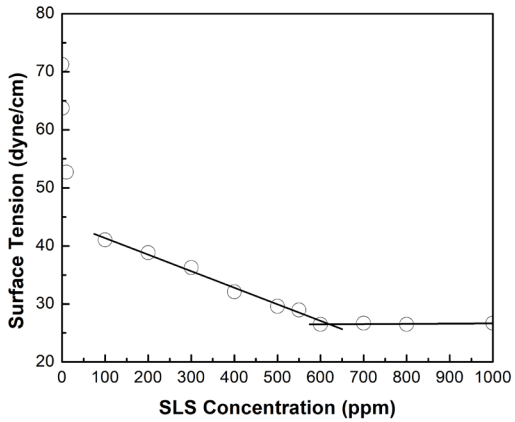

Fig. 3 The surface tension of SLS solution at various concentrations to determine the CMC value

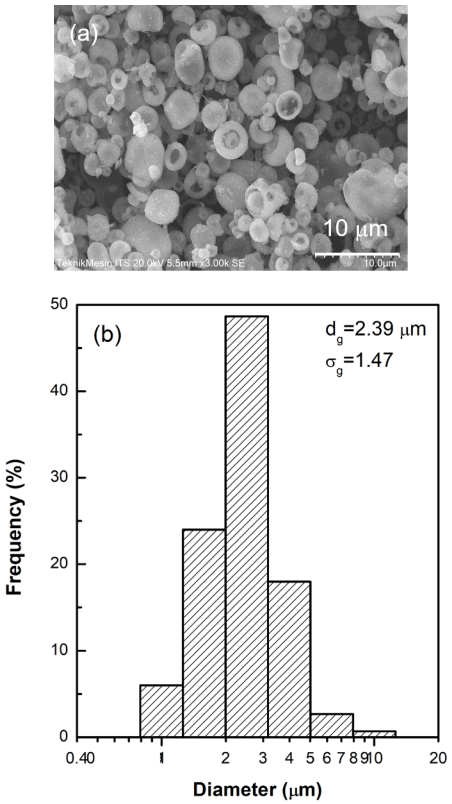

Fig. 4 (a) The SEM image and (b) the particle size distribution of silica particles with SLS concentration of 0.5 CMC

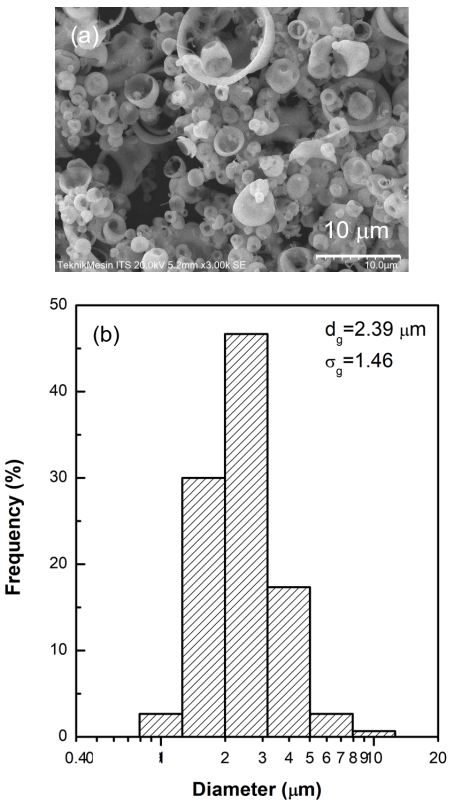

Fig. 5 (a) The SEM image and (b) the particle size distribution of silica particles with SLS concentration of 1 CMC

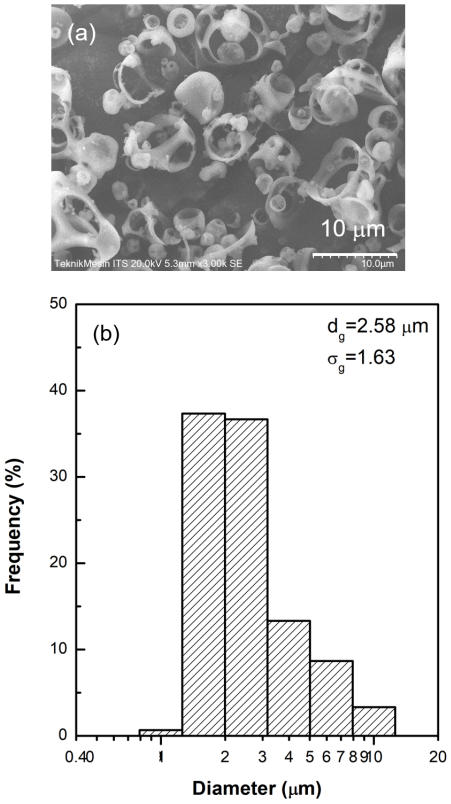

Fig. 6 (a) The SEM image and (b) the particle size distribution of silica particles with SLS concentration of 2 CMC

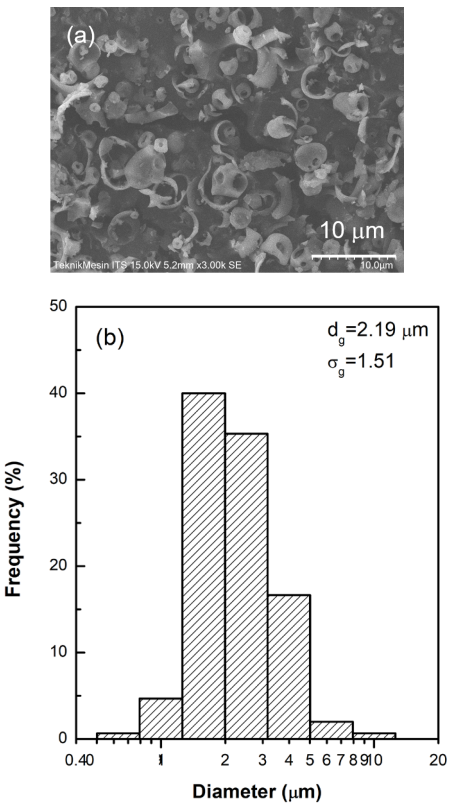

Fig. 7 (a) The SEM image and (b) the particle size distribution of silica particles with SLS template at a concentration of 3 CMC

silica particles with the addition of SLS at a concentration of 0.5 CMC. Although the donut-like particles still tend to be dominant, the SLS concentration of 1 CMC began to show the formation of porous particles. The porous particles formed have a macropore structure with 0.2 to 1.6 μm pore sizes. The formation of pores on silica particles occurs due to the decomposition of the surfactant molecules (micelles) aggregation during the spray drying process.

Besides morphology, the resulting particle's uniformity is also one of the most critical parameters in the synthesis of silica particles. Particle uniformity is defined as the polydispersity index (PdI), which is the result of a comparison between the standard deviation of the particle size distribution (σ) and the mean particle diameter (d_g). If a sample has a PdI less than 0.1, it can be stated that the particles have a uniform distribution (monodisperse), while the PdI is more than 0.1, the particles have a non-uniform distribution (polydisperse) [38]. For example, silica particles without the addition of SLS have a PdI of 0.1235, which indicates that the particle size distribution is not uniform. In contrast, particles synthesized with SLS at concentrations of 0.5 and 1 CMC have PdI of 0.0946 and 0.0933, respectively, showing a uniform particle size distribution.

A significant change occurred when the surfactant concentration was increased to 2 CMC, as shown in Fig. 6 (a). A macro-pore structure is formed in the silica particles. Besides that, the distance between the pores is getting narrower. The macropore structure has a larger size than silica particles with SLS at a concentration of 1 CMC and has a broader range with a pore size of 0.7 to 9.8 μm. The significant change in silica particles is due to the surfactant acting as a template. Surfactants can form micelles with certain formations after passing their CMC values. When the precursor solution is sprayed at a high temperature, the solvent evaporates fast, causing particle shrinkage. It makes the decrease in droplet volume and the increase in solute concentration. The decrease in droplet volume causes the formation of aggregation between silica nanoparticles and micelles. Besides solvent evaporation, the decomposition of surfactant molecules occurred due to high temperatures during the spray drying process. As a result, the micelles will disappear with solvent vapor and leave a pore structure on the particles. The results above indicate that the resulting micellar formation tends to be spherical with relatively symmetrical (round) holes. The number of micelles causes the distance between micelles to get closer so that the space available for nucleation of silica molecules becomes relatively limited and causes the resulting silica particle's wall to become thinner with increasing surfactant concentration. The change in the silica particle's size at a concentration of 2 CMC also increased at an average of 2.58 μm, as shown in Fig. 6 (b). The silica particles with the SLS concentration of 2 CMC show a PdI of 0.0998, indicating the uniform silica particle size distribution.

Fig. 7 (a) shows the morphology of silica particles when the SLS concentration of 3 CMC. The resulting particles show irregular morphology, which tends to be in the form of flakes. However, some particles still have smaller macropore structures than silica particles with the SLS concentration of 2 CMC, with pore sizes of 0.2 to 1.6 μm. A concentration of 3 CMC showed a brittle structure caused by the increasing number of micelles formed in the droplets so that the space available for silica nucleation decreased. As with the SLS concentration of 2 CMC, at the SLS concentration of 3 CMC, it is more likely that the micelles would combine and form more giant micelles. Therefore, the greater the concentration of surfactant added to the silica matrix causes a decrease in the silica fraction due to the increasing number of micelles formed in the droplets. Fig. 7 (b) shows that the size of the silica particles has decreased to 2.19 μm. The SLS concentration of 3 CMC has a PdI of 0.1188, which indicates a non-uniform particle size distribution. The addition of SLS as a template in the synthesis of silica particles can increase the particle size distribution uniformity. However, as they have exceeded a particular SLS concentration, the particle size distribution has a polydisperse pattern that led to PdI increase.

The mechanism for the formation of porous particles is illustrated in Fig. 8. When the surfactants dissolve in water, they form micelles as the SLS concentration increases. The hydrophilic surfactants at the head group will be immobilized on the silica surface by forming physical bonds. Meanwhile, the hydrophobic group of the surfactant molecule will meet the hydrophobic group of other surfactant molecules and form a particular formation. The particle formation in the droplet during the spray process depends on the SLS concentration. When the drying process takes place at high temperatures, the micellar formation will decompose and cause the formation of a pore structure on the silica surface. The morphology of the silica particles produced is influenced by the concentration of surfactants in the silica matrix. The higher the surfactant concentration, the higher the micelle fraction in a droplet. The use of high surfactant concentration led the silica particles to brittle due to the limited space available for silica nanoparticles between micelles.

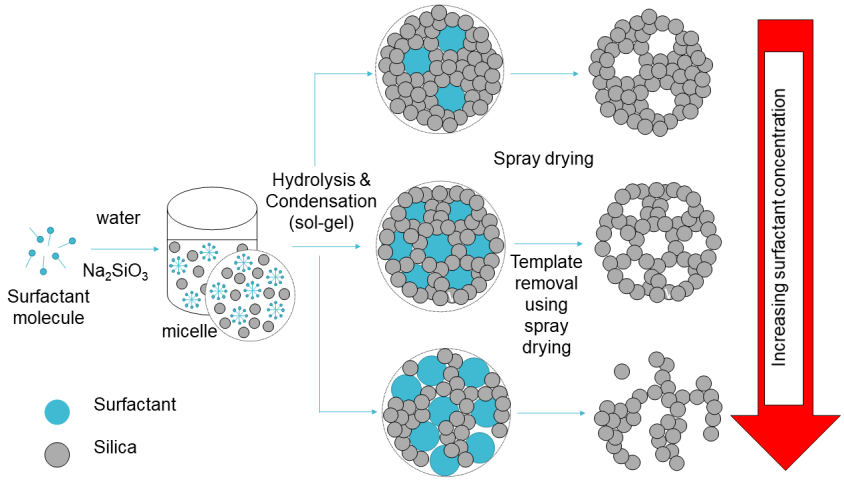

Fig. 8 The mechanism of the porous material formation using a surfactant template

Fig. 9 shows the FTIR spectra of the silica nanofluid as a precursor-surfactant solution and surfactant-template silica particles. Both spectra show a difference between silica nanofluid and silica particles at the wavenumber of 3,331 and 1,636 cm^{-1}, an intramolecular hydrogen bond (O-H stretching) of water molecules. However, the intramolecular hydrogen bond disappears in the silica particles spectra after the drying process. In addition, the presence of intense transmittances shows the characteristic of silica only, whereas the chemical bond identified as surfactant disappears. These results indicate that the release of physical bonds between the surfactant and silica due to high drying temperatures causes the surfactants to decompose and form the pore structure, as shown in the SEM images. Furthermore, the intense transmittance varied in silica or Si-O-Si bond at the wavenumber of 1,061 cm^{-1}. In addition, the peak at the wavenumbers of 459 and 448 cm^{-1} attributed to a Si-O-Si or O-Si-O bond in SiO_2. The rise at a defined peak of 2,340 to 2,360 cm^{-1} indicates the fundamental O-H stretching. The bond is commonly observed in alkaline silicates.

Fig. 10 (a) shows the profile of N_2 adsorption-desorption analysis with various SLS concentrations. There are the same curves as shown by silica particles with and without SLS anionic surfactants as templates. Silica particles

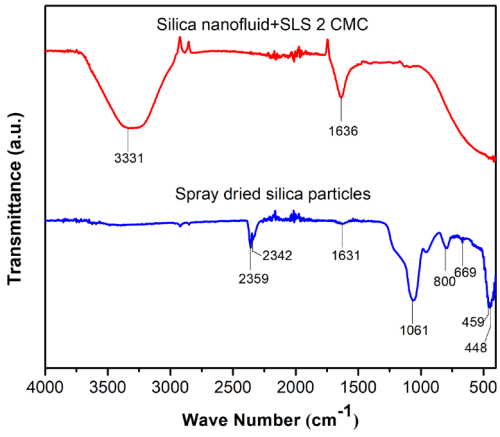

Fig. 9 FTIR spectra of silica nanofluid and silica particles with SLS template

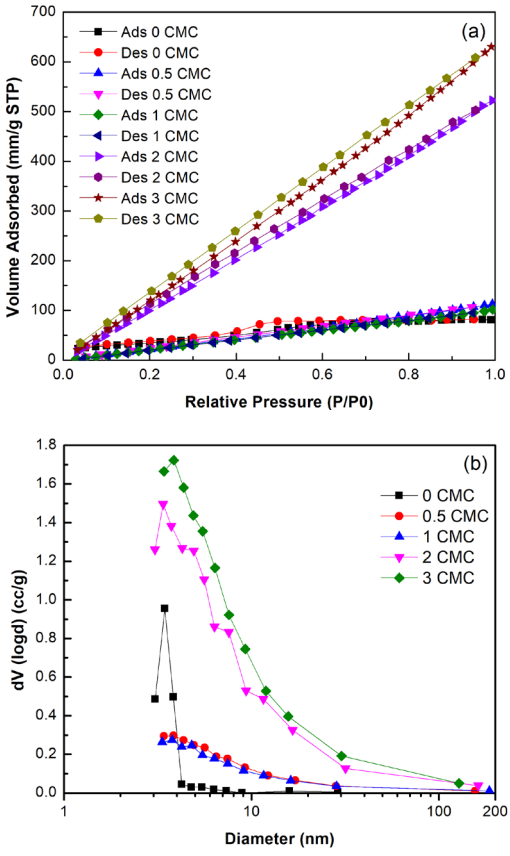

Fig. 10 (a) N_2 adsorption-desorption isotherm and (b) Mesopore size distribution of silica particles at a various surfactant concentration

with various concentrations of SLS show an N_2 type IV adsorption curve. It is characterized by a particular characteristic: a hysteresis loop associated with capillary condensation that occurs in mesoporous. The absorption is limited to high P/Po distance. The initial part of the type IV curve corresponds to the multilayer-monolayer linear adsorption. It indicates that the single layer adsorption stage has been completed and the multilayer stage begins. The type of hysteresis H2, an intermediary for H1 and H4, is caused by differences in condensation and evaporation mechanisms in pores with narrow necks and broad bodies. On type IV of adsorption-desorption N_2 curve is indicated by the presence of hysteresis in the curve, which means mesoporous structures in the material. In the SEM image, it is clear that the silica particles have a macropore structure formed due to the removal of the template formed by the aggregation of surfactant molecules or micellar. However, this adsorption-desorption profile also shows a mesoporous structure with an average pore diameter of around 3 nm. Therefore, it seems that the mesoporous structure is formed from the polymerization of silica during the hydration and condensation (sol-gel) process, which is also shown in silica particles without the SLS addition.

The BJH pore size analysis is carried out to investigate the pore size distribution further to show the differential pore volume versus pore diameter, as indicated in Fig. 10 (b). The pore size distribution for silica particles without SLS addition shows the narrow with more than 50% of mesopore volume located within 3–4 nm pores, and the rest are not more than 12 nm, which still categories mesopore particles. On the contrary, in the case of silica particles with SLS addition, the most volume is occupied by pore size in the range of 3–4 nm. For SLS concentrations of 0.5, 1, and 2 CMC, the mesopore size with a pore size less than 50 nm occupies volume at around 60% volume, and the rest are macropore size with the pore size larger than 50 nm. However, when the concentration of SLS is increased to 3 CMC, the occupied volume by mesopore size increases to 68% volume. It correlates with the SEM images that most particles broken up into fractal particles led to a decrease in volume number of macropore size.

The average pore size, the total pore volume, and the specific surface area are summarized in Table 1. The average mesopore sizes for silica particles generated by varied SLS addition in the precursor are almost the same in the range of 3–4 nm. On the other hand, the total pore volume slightly increases for silica particles synthesized using the SLS concentration of 0.5 CMC compared to without SLS addition. Thus, a significant increase in total pore volume

Table 1 Specific surface area and particle porosity parameters

SLS concentration (CMC)	Average pore size (nm)	Total pore volume (cm^3/g)	Specific surface area (m^2/g)
0	3.82 ± 0.28	0.1251 ± 0.01	131.001
0.5	3.83 ± 0.20	0.1741 ± 0.01	181.603
1	3.06 ± 0.38	0.1573 ± 0.01	205.652
2	3.78 ± 0.19	0.8080 ± 0.03	854.108
3	3.86 ± 0.21	0.9751 ± 0.05	1,011.443

is obtained for silica particles synthesized using the SLS concentration of 2 CMC, around eight higher volumes than without SLS addition. The highest total pore volume is 0.9751 cm^3/g obtained for silica particles synthesized using the SLS concentration of 3 CMC. The increase in a specific surface area correlates with the increase in total pore volume, which a significant increase is obtained for silica particles synthesized using at least at the SLS concentration of 2 CMC. Silica particles synthesized using the SLS concentration of 3 CMC have the largest specific surface area reaching 1,011 m^2/g. Therefore, the addition of SLS at least at 2 CMC or higher leads to a significant increase in total pore volume and the specific surface area because the micelle formation is enough for sacrificed template formation.

The type IV of N_2 adsorption-desorption isotherm curve with hysteresis showing mesoporous characteristics was also confirmed by XRD analysis. Fig. 11 shows the X-ray diffraction analysis of silica particles using an SLS concentration of 2 CMC. The analysis results identified that silica has the characteristics of a porous material with an amorphous structure. It can be seen from the sloping peak at $2\theta = 22–26$ that the degree of crystallinity is 39.7%.

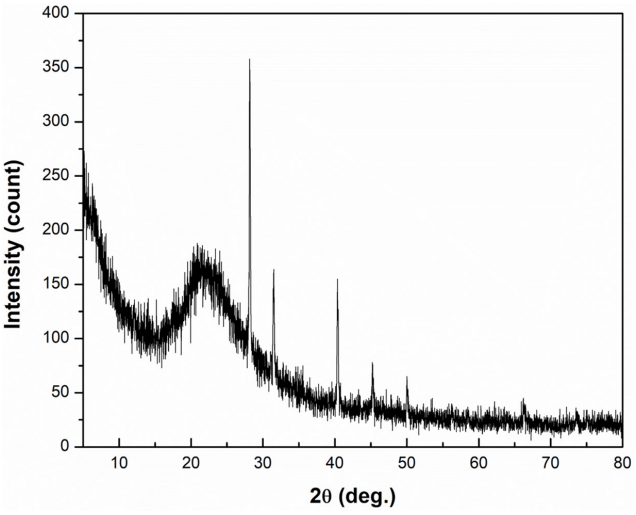

Fig. 11 XRD pattern of silica particles with SLS template at a concentration of 2 CMC

Due to the high surface area and total pore volume, the synthesized silica particles were further evaluated for their performance as adsorbents for dye removal. Silica particles used as adsorbents consisted of four different template concentrations: silica particles without and with SLS template at concentrations of 1, 2, and 3 CMC. Fig. 12 shows the relationship curve between C_e (mg/L) and Q_e (mg/g) obtained from experimental data and fitted to the Langmuir model. The experimental data for isothermal adsorption is obtained from decreasing the concentration of methylene blue as a model of dye waste with variations in the initial concentration. The Langmuir isothermal adsorption parameters obtained from Eq. (2) are shown in Table 2. The theoretical maximum monolayer adsorption capacity shown by each adsorbent correlates with the specific surface area of the silica particles. The higher the surface area, the higher the theoretical maximum monolayer adsorption capacity. The highest theoretical maximum monolayer adsorption capacity was 142.9 mg/g obtained for the silica adsorbent with SLS at 3 CMC. Decreasing the surface area of the adsorbent gives a lower theoretical maximum monolayer adsorption capacity. The silica adsorbent with the SLS template at a concentration of 2 CMC, 1 CMC, and without the SLS template were 82.0, 31.8, and 20.5 mg/g, respectively. The theoretical

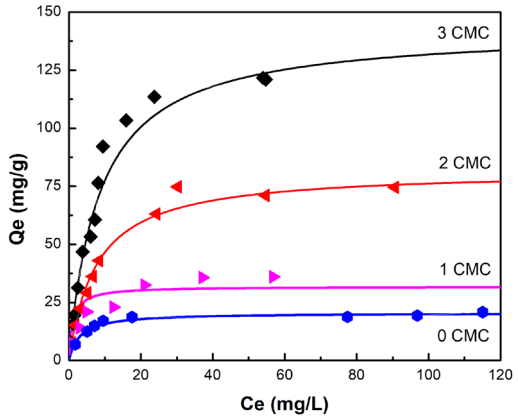

Fig. 12 The adsorption capacity of silica particles without and with SLS template at various concentration

Table 2 Parameters of Langmuir adsorption isotherms at 30 °C for silica particles without and with SLS template at various concentration

SLS concentration (CMC)	Q_m (mg/g)	k	R^2
0	20.5	0.3338	0.997
1	31.8	0.9318	0.996
2	82.0	0.1317	0.996
3	142.9	0.1186	0.991

maximum monolayer adsorption capacity of silica adsorbent synthesized using SLS concentration of 3 CMC shows a higher value than previous studies of silica gel synthesized from coal fly ash and silica-coated magnetite of 23.31 and 24.21 mg/g, respectively [2, 39]. In this case, the adsorption ability of silica particles using the SLS template at a concentration of 3 CMC was almost the same with activated carbon nanofiber without further treatment, which was 149.3 mg/g with the specific surface area of 1,093.845 m^2/g [40].

4 Conclusions

The silica particle was successfully synthesized in a one-step spray drying method followed by template removal of SLS surfactant. An increase in SLS concentration as a template indicates an increase in the size of the resulting silica particles. The higher the surfactant concentration up to 2 CMC can increase the silica particle size from 2.12 µm without a template to 2.58 µm. On the other hand, when the surfactant concentration increases to 3 CMC, the particle size decreases to 2.19 µm with irregular shape and has a brittle structure. The silica particle synthesized without surfactant has a 131 m^2/g specific surface area and a 0.1251 cm^3/g total pore volume. The addition of the surfactant increases the specific surface area as high as 1,011 m^2/g and the total pore volume as high as 0.9751 cm^3/g for silica particles synthesized using the SLS concentration of 3 CMC. However, the structure of silica particles tended to break easily. Thus, the surfactant can increase the surface area of silica particles and make a macrostructure generated by the interaction of aggregation surfactant molecules or micelle. The adsorption mechanism of the silica adsorbent follows the Langmuir isothermal adsorption model. The highest adsorption capacity was obtained at 142.9 mg/g by the silica particles with an SLS template at a concentration of 3 CMC.

Acknowledgment

We would like to thank Deputy for Strengthening Research and Development, the Ministry of Research and Technology/National Research and Innovation Agency, Indonesia, through Applied Research Grant for funding this research (derivate contract no. 995/PKS/ITS/2021).

Nomenclature

ASTM American Society for Testing and Material
C_i initial concentration
C_e equilibrium concentration

CMC	Critical Micelle Concentration
d_g	mean particle diameter
k	Langmuir constant
m	mass
µm	micrometer
nm	nanometer
PdI	Polydispersity Index
SLS	Sodium Lauryl Sulfate
Q_e	equilibrium capacity
Q_m	theoretical maximum monolayer adsorption capacity
V	volume
σ	standart deviation

References

[1] Sun, B., Zhou, G., Zhang, H. "Synthesis, functionalization, and applications of morphology-controllable silica-based nanostructures: A review", Progress in Solid State Chemistry, 44(1), pp. 1–19, 2016. https://doi.org/10.1016/j.progsolidstchem.2016.01.001

[2] Sulistiyo, Y. A., Andriana, N., Piluharto, B., Zulfikar, Z. "Silica Gels from Coal Fly Ash as Methylene Blue Adsorbent: Isotherm and Kinetic Studies", Bulletin of Chemical Reaction Engineering and Catalysis, 12(2), pp. 263–272, 2017. https://doi.org/10.9767/bcrec.12.2.766.263-272

[3] Qiao, B., Wang, T. J., Gao, H., Jin, Y. "High density silanization of nano-silica particles using γ-aminopropyltriethoxysilane (APTES)", Applied Surface Science, 351, pp. 646–654, 2015. https://doi.org/10.1016/j.apsusc.2015.05.174

[4] Huang, H. Y., Yang, R. T., Chinn, D., Munson, C. L. "Amine-grafted MCM-48 and Silica Xerogel as Superior Sorbents for Acidic Gas Removal from Natural Gas", Industrial and Engineering Chemistry Research, 42(12), pp. 2427–2433, 2003. https://doi.org/10.1021/ie020440u

[5] Li, X., Xiong, Y., Chen, D., Zou, C. "Utilization of nanoparticle-stabilized foam for gas well deliquification", Colloids and Surfaces A: Physicochemical and Engineering Aspects, 482, pp. 378–385, 2015. https://doi.org/10.1016/j.colsurfa.2015.05.053

[6] Wu, J., Lei, Q., Xiong, C., Cao, G., Zhang, J., Li, J., Fanf, J., Tan, J., Ai, T., Li, N., Jia, M. "A nanoparticle foam unloading agent applied in unloading liquid of deep gas well", Petroleum Exploration and Development, 43(4), pp. 695–700, 2016. https://doi.org/10.1016/S1876-3804(16)30081-7

[7] Su, M., Su, H., Ren, G., Du, B., Li, X., Wang, S. "Effect of drying technique on the morphological and textural characteristics of mesoporous silica synthesized in the microreactor", Journal of Sol-Gel Science and Technology, 73(2), pp. 460–468, 2015. https://doi.org/10.1007/s10971-014-3562-7

[8] Wang, B., Friess, W. "Spray drying of silica microparticles for sustained release application with a new sol-gel precursor", International Journal of Pharmaceutics, 532(1), pp. 281–288, 2017. https://doi.org/10.1016/j.ijpharm.2017.09.016

[9] Muljani, S., Setyawan, H., Wibawa, G., Altway, A. "A facile method for the production of high-surface-area mesoporous silica gels from geothermal sludge", Advanced Powder Technology, 25(5), pp. 1593–1599, 2014. https://doi.org/10.1016/j.apt.2014.05.012

[10] Nazriati, N., Setyawan, H., Affandi, S., Yuwana, M., Winardi, S. "Using bagasse ash as a silica source when preparing silica aerogels via ambient pressure drying", Journal of Non-Crystalline Solids, 400, pp. 6–11, 2014. https://doi.org/10.1016/j.jnoncrysol.2014.04.027

[11] Cho, K., Chang, H., Kil, D. S., Park, J., Jang, H. D., Sohn, H. Y. "Mechanisms of the formation of silica particles from precursors with different volatilities by flame spray pyrolysis", Aerosol Science Technology, 43(9), pp. 911–920, 2009. https://doi.org/10.1080/02786820903025986

[12] Santamaría, E., Maestro, A., Porras, M., Gutiérrez, J. M, González, C. "Preparation of structured meso-macroporous silica materials: Influence of composition variables on material characteristics", Journal of Porous Materials, 21(3), pp. 263–274, 2014. https://doi.org/10.1007/s10934-013-9771-6

[13] Rahman, N. A., Widhiana, I., Juliastuti, S. R., Setyawan, H. "Synthesis of mesoporous silica with controlled pore structure from bagasse ash as a silica source", Colloids and Surfaces A: Physicochemical Engineering Aspects, 476, pp. 1–7, 2015. https://doi.org/10.1016/j.colsurfa.2015.03.018

[14] Lee, S. G., Jang, Y. S., Park, S. S., Kang, B. S., Moon, B. Y., Park, H. C. "Synthesis of fine sodium-free silica powder from sodium silicate using w/o emulsion", Materials Chemistry and Physics, 100(2–3), pp. 503–506, 2006. https://doi.org/10.1016/j.matchemphys.2006.02.001

[15] Zhang, S.-W., Zhou, S.-X., Weng, Y.-M., Wu, L.-M. "Synthesis of SiO_2/Polystyrene Nanocomposite Particles via Miniemulsion Polymerization", Langmuir, 21(6), pp. 2124–2128, 2005. https://doi.org/10.1021/la047652b

[16] Qomariyah, L., Arif, A. F., Widiyastuti, W., Winardi, S., Taniguchi, S., Ogi, T. "Hexagonal hollow silica plate particles with high transmittance under ultraviolet-visible light", RSC Advances, 8(46), pp. 26277–26282, 2018. https://doi.org/10.1039/C8RA04787A

[17] Zulfiqar, U., Subhani, T., Husain, S. W. "Synthesis of silica nanoparticles from sodium silicate under alkaline conditions", Journal of Sol-Gel Science Technology, 77(3), pp. 753–758, 2016. https://doi.org/10.1007/s10971-015-3950-7

[18] Trewyn, B. G., Slowing, I. I., Giri, S., Chen, H. T., Lin, V. S.-Y. "Synthesis and Functionalization of a Mesoporous Silica Nanoparticle Based on the Sol-Gel Process and Applications in Controlled Release", Accounts of Chemical Research, 40(9), pp. 846–853, 2007. https://doi.org/10.1021/ar600032u

[19] Qomariyah, L., Widiyastuti, W., Winardi, S. "Effect of colloidal properties on the particle characteristics in the flame-assisted spray-drying process", Chemical Papers, 74(1), pp. 285–296, 2020. https://doi.org/10.1007/s11696-019-00878-8

[20] Qomariyah, L., Widiyastuti, W., Winardi, S., Kusdianto, K., Ogi, T. "Volume Fraction Dependent Morphological Transition of Silica Particles Derived from Sodium Silicate", International Journal of Technology, 10(3), 2019. https://doi.org/10.14716/ijtech.v10i3.2917

[21] Lee, S. Y., Widiyastuti, W., Iskandar, F., Okuyama, K., Gradoń, L. "Morphology and Particle Size Distribution Controls of Droplet-to-Macroporous/Hollow Particles Formation in Spray Drying Process of Colloidal Mixtures Precursor", Aerosol Science and Technology, 43(12), pp. 1184–1191, 2009. https://doi.org/10.1080/02786820903277553

[22] Nandiyanto, A. B. D., Okuyama, K. "Progress in developing spray-drying methods for the production of controlled morphology particles: From the nanometer to submicrometer size ranges", Advanced Powder Technology, 22,(1), pp. 1–19, 2011. https://doi.org/10.1016/j.apt.2010.09.011

[23] Bao, Y., Shi, C., Wang, T., Li, X., Ma, J. "Recent progress in hollow silica: Template synthesis, morphologies and applications", Microporous and Mesoporous Materials, 227, pp. 121–136, 2016. https://doi.org/10.1016/j.micromeso.2016.02.040

[24] Kamyabi, M. A., Ebrahimi-Qaratapeh, K., Moharramnezhad, M. "Silica template as a morphology-controlling agent for deposition of platinum nanostructure on 3D-Ni-foam and its superior electrocatalytic performance towards methanol oxidation", Journal of Porous Materials, 28(2), pp. 393–405, 2021. https://doi.org/10.1007/s10934-020-01001-z

[25] Lee, S. Y., Widiyastuti, W., Tajima, N., Iskandar, F., Okuyama, K. "Measurement of the Effective Density of Both Spherical Aggregated and Ordered Porous Aerosol Particles Using Mobility- and Mass-Analyzers", Aerosol Science and Technology, 43(2), pp. 136–144, 2009. https://doi.org/10.1080/02786820802530524

[26] Winardi, S., Qomariyah, L., Widiyastuti, W., Kusdianto, K., Nurtono, T., Madhania, S. "The role of electro-sprayed silica-coated zinc oxide nanoparticles to hollow silica nanoparticles for optical devices material and their characterization", Colloids and Surfaces A: Physicochemical and Engineering Aspects, 604, Article number: 125327, 2020. https://doi.org/10.1016/j.colsurfa.2020.125327

[27] Okuyama, K., Abdullah, M., Lenggoro, I. W., Iskandar, F. "Preparation of functional nanostructured particles by spray drying", Advanced Powder Technology, 17(6), pp. 587–611, 2006. https://doi.org/10.1163/156855206778917733

[28] Fameau, A.-L., Salonen, A. "Effect of particles and aggregated structures on the foam stability and aging", Comptes Rendus Physique, 15(8–9), pp. 748–760, 2014. https://doi.org/10.1016/j.crhy.2014.09.009

[29] Zulfajri, M., Huang, W.-J., Huang, G.-G., Chen, H.-F. "Effects of Different Surfactant Charges on the Formation of Gold Nanoparticles by the LASiS Method", Materials, 14(11), Article number: 2937, 2021. https://doi.org/10.3390/ma14112937

[30] Nagappan, S., Mohan, A., Thomas, A. M., Yoo, J.-M., Eid, N., Chung, I., Ameduri, B., Ha, C.-S. "Synthesis of size-controlled and highly monodispersed silica nanoparticles using a short alkyl-chain fluorinated surfactant", RSC Advances, 11(4), pp. 2194–2201, 2021. https://doi.org/10.1039/D0RA08114K

[31] Eftekhari, M., Schwarzenberger, K., Javadi, A., Eckert, K. "The influence of negatively charged silica nanoparticles on the surface properties of anionic surfactants: electrostatic repulsion or the effect of ionic strength?", Physical Chemistry Chemical Physics, 22(4), pp. 2238–2248, 2020. https://doi.org/10.1039/C9CP05475H

[32] Lin, H.-P., Mou, C.-Y. "Structural and Morphological Control of Cationic Surfactant-Templated Mesoporous Silica", Accounts of Chemical Research, 35(11), pp. 927–935, 2002. https://doi.org/10.1021/ar000074f

[33] Ui, S.-W., Choi, I.-S., Choi, S.-C. "Synthesis of High Surface Area Mesoporous Silica Powder Using Anionic Surfactant", ISRN Materials Science, 2014, Article ID: 834629, 2014. https://doi.org/10.1155/2014/834629

[34] Yokoi, T., Tatsumi, T. "Synthesis of Mesoporous Silica Materials by Using Anionic Surfactants as Template", Journal of the Japan Petroleum Institute, 50(6), pp. 299–311, 2007. https://doi.org/10.1627/jpi.50.299

[35] Hashimoto, K., Masuda, T. "Change in surface area of silica-alumina catalysts caused by sintering in steam atmosphere", Journal of Chemical Engineering of Japan, 18(1), pp. 71–78, 1985. https://doi.org/10.1252/jcej.18.71

[36] Han, Y. S., Li, J. B., Chi, B., Wen, Z. W. "The Effect of Sintering Temperature on Porous Silica Composite Strength", Journal of Porous Materials, 10(1), pp. 41–45, 2003. https://doi.org/10.1023/A:1024070114030

[37] Qomariyah, L., Sasmita, F. N., Novaldi, H. R., Widiyastuti, W., Winardi, S. "Preparation of Stable Colloidal Silica with Controlled Size Nano Spheres from Sodium Silicate Solution", IOP Conference Series: Materials Science and Engineering, 395, Article number: 012017, 2018. https://doi.org/10.1088/1757-899X/395/1/012017

[38] Clayton, K. N., Salameh, J. W., Wereley, S. T., Kinzer-Ursem, T. L. "Physical characterization of nanoparticle size and surface modification using particle scattering diffusometry", Biomicrofluidics, 10(5), Article number: 054107, 2016. https://doi.org/10.1063/1.4962992

[39] Setyawan, H., Widiyastuti, W., Mahmudi, M., Dian Pusfitasari, M. "Silica-coated Magnetite Nanoparticles Prepared by the One-step Electrochemical Method for Dye Removal", Journal of Powder Technology and Advanced Functional Materials, 1(1), pp. 1–11, 2018. https://doi.org/10.29253/jptafm.1.1.2018.1

[40] Widiyastuti, W., Fahrudin Rois, M., Suari, N. M. I. P., Setyawan, H. "Activated carbon nanofibers derived from coconut shell charcoal for dye removal application", Advanced Powder Technology, 31(8), pp. 3267–3273, 2020. https://doi.org/10.1016/j.apt.2020.06.012